STATISTICS OF SCALAR FIELDS IN THE ATMOSPHERIC BOUNDARY LAYER BASED ON LARGE-EDDY SIMULATIONS. PART II: FORCED CONVECTION

Zbigniew Sorbjan

Department of Physics, Marquette University, Milwaukee, WI 53201, U.S.A.

address:

Marquette University, Department of Physics

Wehr Phys. Bld., Room 377

540 North 15th Street, Milwaukee, WI 53201-1881

tel, (414) 288-7458, or (414) 288-7458

fax: (414) 288-3989, e-mail: sorbjanz@mu.edu

Accepted to "Boundary-Layer Meteorology", ref: BOUN2477-04D

First draft: August 16, 2004, Final draft on March 20, 2005

Abstract. Forced convection in a quasi-steady atmospheric boundary layer is investigated based on a large-eddy simulation (LES) model. The performed simulations show that in the upper portion of the mixed layer the dimensionless (in terms of mixed layer) vertical gradients of temperature, humidity, and wind velocity depend on the dimensionless height z/z_i and the Reech number Rn. The characteristic (peak) values of variances and covariances at the top of the mixed layer, scaled in terms of the interfacial scales, are functions of the interfacial Richardson number Ri. Profiles of dimensionless scalar moments in the mixed layer are proposed to be expressed in terms of two empirical similarity functions F_m and F_i, dependent on dimensionless height z/z_i, and the interfacial Richardson number Ri. The obtained similarity expressions adequately approximate the LES profiles of scalar statistics, and properly represent the impact of stability, shear, and entrainment. They are also consistent with the parameterization proposed for free convection in the first part of this paper.

Keywords: Atmospheric boundary layer, Forced-convection, Interfacial layer, Entrainment, Large-eddy simulations, Similarity scales

1. Introduction

The convective atmospheric boundary layer (ABL) has a multi-layer structure. It consists of the surface layer, near the Earth's surface, the mixed layer above, and the interfacial layer at the top. Both, the surface layer and the mixed layer have been intensively studied during the last five decades (e.g., Garratt, 1992). The interfacial layer, and its impact on boundary-layer convection, has obtained relatively less theoretical attention (e.g., Otte and Wyngaard, 2000; Sorbjan, 2001; Sorbjan, 2004).

In order to develop a better understanding of the interfacial layer and its role on the mixed layer, a two-part numerical study has been performed. Its Part I (Sorbjan, 2005) focused on free convection. The present paper (which constitutes the second part of the study) is devoted to investigate forced convection. In both parts, the large-eddy simulation (LES) model of Sorbjan (1996) has been used as a research tool, due to its ability to generate various flow regimes, test theories, and evaluate parameterizations of the ABL.

As discussed in Part I, free convection refers to calm conditions. Its presence in the boundary layer can be identified with horizontally hexagonal cells (e.g., Moeng and Sullivan, 1994). Turbulence in this case is controlled only by the strength of the surface heat flux. In the surface layer, it can be described in terms of free-convection scales for vertical velocity, temperature, humidity (or other passive scalar), and height (Wyngaard et al., 1971):

$$u_f = (\beta\, z\, H_o)^{1/3}, \qquad \Theta_* = H_o/w_*, \qquad q_* = Q_o/w_*\,, \qquad z \tag{1}$$

where H_o is the surface virtual potential temperature flux, Q_o is a scalar flux (of water vapor, carbon dioxide, ozone, methane, nitrogen oxides, etc), $\beta = g/T_o$ is the buoyancy parameter. In the mixed layer, characteristics of turbulence can be expressed in terms of the convective scales (Deardorff, 1970):

$$w_* = (\beta\, z_i\, H_o)^{1/3}, \qquad \Theta_* = H_o/w_*, \qquad q_* = Q_o/w_*, \qquad z_i \tag{2}$$

where z_i is defined here as the level at which the heat flux H(z) is most negative. The mixed layer scales have been applied both in shear-free and shear conditions.

In the interfacial layer, turbulence can be represented by the interfacial scales (Sorbjan, 2004):

$$S_w = w_*, \qquad S_\theta = \gamma_i\, w_*/N_i, \qquad S_q = g_i\, w_*/N_i, \qquad S_h = w_*/N_i \tag{3}$$

where $N_i = (\beta \gamma_i)^{0.5}$ is the Brunt-Väisäla frequency in the interfacial layer, γ_i is the peak potential (virtual) temperature gradient in the interfacial layer, and g_i is the peak scalar gradient in the interfacial layer.

The fact that two different similarity regimes, expressed by two different sets of scales (2) and (3), are present above the surface layer, causes that statistical moments (fluxes, variances, and covariances) in the shear-less mixed layer can be written in the following form (Sorbjan, 2004, 2005):

$$M = S_m F_m (z/z_i) + S_i F_i (z/z_i) \tag{4}$$

where M is a statistical moment, S_m is a product of the convective scales (2), S_i is a product of the interfacial scales (3), and F_m, F_i are empirical functions of dimensionless height z/z_i. The form of F_m and F_i was proposed in Part I. Generally, F_m is a decreasing function of height, reaching zero at the top of the mixed layer. F_i is an increasing function of z/z_i, approaching a universal constant at the top of the mixed layer. In the surface layer, F_m is expected to match the Monin-Obukhov predictions.

Forced convection refers to windy conditions. Its presence in the boundary layer can be identified with characteristic horizontal roll vortices (e.g., Moeng and Sullivan, 1994, Glendening, 1996, Kim et al., 2003). During forced convection, turbulence is controlled not only by the strength of the surface heat flux, but also by wind shear. Equation (4) is generally not valid, because, the statistics of turbulence at the top of the mixed layer depend not only on the temperature gradient γ_i, but also on the velocity gradients $s_{xi} = du/dzl_i$ and $s_{yi} = dv/dzl_i$ in the interfacial layer, or equivalently on the interfacial Richardson number $Ri = N_i^2/s_i^2$, where $s_i^2 = s_{xi}^2 + s_{yi}^2$. Consequently, (4) could be replaced by the following expression (Sorbjan, 2004):

$$M = S_m F_m (z/z_i) + S_i F_i (z/z_i, 1/Ri) \quad (5)$$

which is formally valid only above the surface layer, since F_m is a function of a single parameter z/z_i (i.e., it is independent of z_i/L, where L is the Monin-Obukhov length). It can be assumed that $F_i (z/z_i, 1/Ri) = F_1(z/z_i) F_2(1/Ri)$, and that $F_2(1/Ri) \rightarrow 1$, when $1/Ri \rightarrow 0$. As a result, in the shear-less case ($1/Ri = 0$), Equation (5) coincides with (4). The dependence of functions F_i on Ri, for fluxes, variances, and covariances at the top of the mixed layer, was proposed by Sorbjan (2004, 2005).

In Part I of this paper, numerical tests of Equation (4) have been carried out in the shear-less case (when $1/Ri = 0$), for various values of the the Brunt-Väisäla frequency N_i. In this paper an examination of Equations (5) will be performed by varying the temperature gradient γ_i, and in addition, by changing the values of the geostrophic wind G. The structure of the paper is as follows. The performed simulations are outlined in Section 2. The obtained results are presented in Section 3. The forced-convection parameterization is introduced in Section 4.

2. Large-Eddy Simulations

Forced convection is numerically more difficult to simulate than its free-convective counterpart (e.g., by Mason, 1992; Moeng and Sullivan, 1994; Glendening, 1996; Kim, et al., 2003; Sorbjan, 2004). The horizontal domain needs to be larger (several times larger that z_i), the simulation time significantly longer, and the time step shorter. The final averaging period has to be sufficiently long, in order to obtain stable statistics of turbulence. Longer averaging, however, causes that the transition between the mixed layer and the free atmosphere is significantly smoothed. This

effect may introduce difficulties in interpretations of the obtained results in the interfacial layer (e.g., Lilly, 2002).

For the purpose of this study, six runs of large-eddy simulation model (Sorbjan, 1996) have been generated. They have been obtained for three values of the geostrophic wind G, and for two values of the temperature gradient γ_i in the interfacial layer. The performed runs will hereafter be referred to as W05, W10, W15, and S05, S10, S15. The letter "W" specifies runs, for which the initial temperature inversion strength γ_i was relatively weak, and equal to 0.01 K m^{-1}. The letter "S" denotes runs with stronger temperature gradients in the interfacial layer, equal to 0.1 K m^{-1}. The numbers 05, 10 and 15 indicate the assumed values of the geostrophic wind G in m s^{-1}.

TABLE 1. Parameters characterizing the simulated cases

Run	Θ_* [K]	q_* [10^{-5}]	w_* [m s^{-1}]	u_* [m s^{-1}]	N_i	z_i [m]	z_i/L	Rn	Ri	T_s [s]
W05	0.059	3.9	1.28	0.263	0.0155	832	-46.3	89.5	10.6	30460.3
S05	0.065	4.3	1.16	0.257	0.0644	619	-36.8	1252.8	52.4	31623.2
W10	0.057	3.8	1.31	0.412	0.0142	880	-12.7	90.9	3.6	33696.1
S10	0.039	5.6	0.89	0. 411	0.0631	590	-4.0	1822.5	15.8	20735.6
W15	0.061	4.1	1.22	0.616	0.0146	716	-3.1	83.5	1.5	14109.6
S15	0.065	4.3	1.15	0.609	0.0644	605	- 2.7	1095.8	6.7	14281.5

The time-averaged characteristics of the performed simulations are summarized in Table 1. Symbols in the table are the same as those used in Equations (1) and (2). In addition, T_s is the time length of each simulation, and Rn is the Reech number, $Rn = (z_i N_i/w_*)^2 = (z_i/S_h)^2$. The

convective scale q_* is the expressed in kg kg^{-1}. The values of the interfacial scales (3) are depicted in Table 2 (note that S_q is also in kg kg^{-1}).

In all of the simulations, the employed mesh consisted of 64 x 64 x 60 grid points. The grid increments were $\Delta x = \Delta y = 40$ m, and $\Delta z = 30$ m. The initial mixed layer was 600 m deep, with a uniformly distributed potential temperature of 299 K. The interfacial layer was initially 150 m thick. In the free-atmosphere, the temperature gradient was assumed to be $\Gamma = 0.003$ K m^{-1}. The initial specific humidity in the mixed layer was equal to 0.010 kg kg^{-1}. It decreased to zero at the top of the interfacial layer. In the free-atmosphere, humidity was assumed to be nil. The roughness parameter was set to equal $z_o = 0.01$ m. The geostrophic wind was aligned with the x-axis. The Coriolis parameter was assumed to be $f = 0.0001$ s^{-1}. The model was initialized assuming the surface heat flux $H_o = 0.075$ K m s^{-1}. The surface scalar (specific humidity) flux Q_o was assumed to be 0.00005 kg kg^{-1}m s^{-1} in all six cases.

TABLE 2. Interfacial layer scales and characteristics in the simulated cases

Run	S_w [m s^{-1}]	S_Θ [K]	S_q [10^{-3}]	S_h [m]	S_Θ/Θ_*	H_i/H_o	S_q/q_*	Q_i/Q_o	humidity trend
W05	1.28	0.56	-4.23	87.7	9.49	-0.15	-108.46	3.40	drying
S05	1.16	2.31	-1.75	17.5	35.54	-0.21	-40.70	0.45	moistening
W10	1.31	0.55	-3.78	92.3	9.65	-0.13	-99.50	3.79	drying
S10	0.89	1.71	-1.13	13.8	43.84	-0.23	-20.17	0.20	moistening
W15	1.22	0.57	-3.60	78.2	9.34	-0.25	-87.80	4.10	drying
S15	1.15	2.18	-1.49	18.3	33.53	-0.33	-34.65	0.45	moistening

All simulations were 10,000 time steps long. Because the time increments during the simulations were automatically adjusted on each time step (based on the Courant-Friedrichs-Levy stability condition), the simulation time T_s was slightly different for each run. The final statistics were obtained through a spatial (horizontal) and temporal averaging during the last 1500 time steps of each simulation (which is equivalent to 735 s in run S15, and 1500 s in run W05). The overturning time scale $\tau_* = z_i/w_*$ varied from 526 s -- in run S15, to 650 s -- in run W05.

3. Results

3.1. PROFILES

The performed simulations were designed to examine the effects of shear and the temperature gradient in the interfacial layer. Figures 1 a-c show the resulting vertical profiles of the potential virtual temperature, humidity (or other passive scalar), and wind velocity components. Two families of temperature profiles are depicted in Figure 1a, one with a small temperature jump in the interfacial layer (runs W05, W10, and W15), and one with a large one (runs S05, S10, and S15).

There are two resulting families of humidity profiles (Figure 1b), as a consequence of the two assumed values of γ_i (the value of the surface humidity flux was the same in all runs). The humidity profiles obtained in runs S05, S10 and S15 converge, while in the remaining W-profiles are more scattered. Profiles W05, W10, and W15 indicate the mixed layer "drying", while in the remaining S cases the "moistening" of the mixed layer takes place. Both regimes were previously discussed by Mahrt (1991).

There are three families of the u-component velocity profiles (Figure 1c), associated with the values of the geostrophic wind, 5, 10 and 15 m s^{-1}. The v-components are nearly the same for all runs, with the mixed layer values of about 0.5 m s^{-1}.

Figures 2 a-c show dimensionless gradient $z_i/\Theta_* \, d\Theta/dz$, obtained in runs: W10, W15, S10, S15 (the runs W05 and S05 are not shown for clarity of the presentation). The temperature gradient in the mixed layer is approximately zero from $z/z_i = 0.2$ up to 0.9 (Figure 2a). The peak values are achieved in the interfacial layer, at about $z/z_i = 1.1$, and are equal to the Reech number, since $z_i\gamma_i/\Theta_* = (z_i/S_h)^2 = Rn$. The dimensionless gradients seem to be independent of the interfacial Richardson number and z_i/L (as it follows from Table 1). Consequently, it can be concluded that the dimensionless gradient in the mixed layer, and above it, is a universal function of only two dimensionless parameters, z/z_i and Rn:

$$z_i/\Theta_* \, d\Theta/dz = F_\theta(z/z_i, Rn) \qquad (6)$$

The same result was obtained in the free-convective case. Note that the above expression is not valid below $z/z_i = 0.2$, because F_θ does not include the parameter z_i/L. For very large N_i, and consequently very small S_h (i.e., infinitesimally shallow interfacial layer), F_θ in (6) is expected to be independent of Rn.

It is worth mentioning that in the free-convective case (Sorbjan, 2005), the Reech was found to be a governing parameter for the mean entrainment rate w_e/w_* (where w_e is the mean temporal growth of the mixed layer depth). The present study indicates that the result obtained in the shearless case, $w_e/w_* = Rn^{-1}$, is also valid during forced convection.

The humidity (scalar) gradient $z_i/q_* \, dq/dz$ is displayed in Figure 2b. The gradient is zero up to $z/z_i = 0.5$ - 0.7, except in run W15. The peak values are reached at about $z/z_i = 1.1$ - 1.2, are about -700 in runs W, and about -1100 in runs S, and are strongly dependent on the temperature gradient γ_i, and equivalently on the Reech number, Rn. Table 1 and the figure indicate that the humidity gradient is independent of the Richardson number Ri, which allows to assume that in the upper part of the mixed layer:

$$z_i/q_* \, dq/dz = F_q(z/z_i, Rn) \qquad (7)$$

The same result was obtained in the free-convective case.

Figure 2c depicts the dimensionless gradient $z_i/u_* \, du/dz$ of the x-component of the wind velocity vector. In the middle of the mixed layer (from $z/z_i = 0.4$ up to 0.7), the dimensionless gradient is near zero. The peak values of the gradient are reached at about $z/z_i = 1.1$. In the interfacial layer, the dimensionless gradient is strongly dependent on the temperature gradient γ_i, and independent on the geostrophic wind G.

Four parameters: u_*, w_*, G, and $N_i z_i$, can be considered as relevant velocity scales in the interfacial layer. Consequently, the dimensionless peak value of the velocity gradient $s_{xi} = du/dz|_i$ could be anticipated to be a function of three products, made from the listed four scales: $z_i \, s_{xi} / u_* = f_u(u_*/G, u_*/w_*, N_i z_i/w_*)$. Table 1 indicates that the ratio $u_*/w_* = (-z_i/L)^{1/3}$ is equal to -9.1 in run W10, -3.1 in run W15, -2.7 in run S10, and -7.7 in run S15 (the equivalent values of $-z_i/L$ are 753.6, 29.8, 19.7, and 456.5 respectively). Taking these values into consideration, we can see in Figure 2c that the dimensionless gradient $z_i/u_* s_{xi}$ is practically independent (in the considered range of $-z_i/L$) of the ratio u_*/w_*. It can also be noticed that the ratio u_*/G is nearly the same in all runs (and equal to 0.0441, 0.0411, 0.0432, 0.0406 in runs W10, W15, S10, and S15

respectively). Since $z_i/u_* s_{xi}$ differs in runs W and S, we conclude that it must be independent of u_*/G. The dimensionless peak value of the velocity gradients, $z_i\ s_{xi}/u_*$ is then expected to be a function of a single parameter $N_i z_i/w_* = z_i/S_h = Rn^{1/2}$. The same conclusion can be applied to the v-component of the wind velocity.

Based on the above discussion, it could be assumed that the dimensionless velocity gradients in the upper half of the (barotropic) convective boundary layer are universal functions of only two dimensionless parameters, z/z_i and Rn:

$$z_i/u_* \, du/dz = F_u(z/z_i, Rn) \qquad (8)$$

$$z_i/u_* \, dv/dz = F_v(z/z_i, Rn)$$

Note that in the lower half of the mixed layer, F_u, and F_v are dependent on z/z_i and z_i/L. For example, in runs W05 and S05, which can be considered as nearly free-convective cases (z_i/L = -46.3 and -36.8), $z_i/u_* \, du/dz$ reaches a zero value at $z/z_i = 0.1$ (much lower than for cases depicted in Figure 2c) and is zero up to about z/z_i = 0.5 - 07 (not shown). From Equations (6) and (8) can also be concluded that the interfacial Richardson number is a function of the Reech number Rn and z_i/L, $Ri = z_i/L \, f(Rn)$.

The second moments of the potential temperature are shown in Figures 3 a-b**.** Figure 3a indicates that the negative peak values of the heat flux H_i increase with the strength of the capping inversion γ_i, and with the value of the geostrophic wind G. The same conclusion applies to the temperature variance σ_θ^2 in Figure 3b (spurious consequences of a sharp temperature gradient are seen in run S15). The dependence of σ_θ^2 on the temperature gradient γ_i is much stronger than the dependence on the geostrophic shear.

Profiles of specific humidity flux, and its variance, are depicted in Figures 4 a-b. It should be remembered that the surface flux Q_o was kept the same in all considered runs, and the variation of the profiles in Figures 4 is only due to the differences in γ_i and G. The flux profiles in Figure 4a are decreasing functions of height in runs S10 and S15. In runs W10 and W15, the humidity flux increases with height. This behavior can be explained (e.g., Deardorff, 1974a) by increasing or decreasing in time (see Figure 1b) specific humidity ("moistening"/("drying") in the mixed layer (note that the initial value of the specific humidity in the mixed layer was 0.01 g kg^{-1} in all runs)

The profiles in Figure 4b reflect sensitivity of σ_q^2 to the strength of the capping inversion γ_i, and the values of the geostrophic wind G. As during free convection, the profiles of humidity variance do not coincide in the surface layer (especially in run W15). A similar result was obtained by Deardorff (1974b), but for weaker wind velocities. The detected departure of the variance profiles indicates that σ_q^2 does not follow the Monin-Obukhov similarity, especially when $Q_i/Q_o > 1$ ("drying"). In Part I, this effect was shown to be accompanied by a low correlation coefficient between temperature and humidity in the surface layer due to entrainment processes. The present study confirms this conclusion. The correlation coefficient (its profile not shown) at $z/z_i = 0.1$ is: 0.35 in run W05, 0.32 in run W10, and 0.50 in run W15 (the "drying" cases, as seen from Figure 1b). In the "moistening" runs, the obtained values of the correlation coefficient are about 0.70 in runs S05, and 0.95 in runs S10, S15.

The second moments of the velocity components are shown in Figures 5 a-b. In the mixed layer, σ_u^2/w_*^2 seems to be independent of γ_i. The horizontal variance σ_u^2/w_*^2 increases, when the geostrophic wind increases. The values of the vertical velocity variances σ_w^2/w_*^2 at the top of the mixed layer increase, when both γ_i and G increase. In Figure 5 b, a deficiency of the sub-grid

scheme can be noticed near the lower surface, due to the fact that in this area the peak in the vertical velocity spectrum is very near to the filter cutoff (Sullivan et al., 2003).

3. 2. THE INTERFACIAL VALUES

The form of the similarity functions F_i (z/z_i=1, Ri) in Eq. 5 was proposed by Sorbjan (2004, 2005):

$$H_i = -c_H S_w S_\theta \ \frac{(1 + c_r / Ri)}{(1 + 1/Ri)^{0.5}} \tag{9a}$$

$$Q_i = -c_Q S_w S_q \ \frac{(1 + c_r / Ri)}{(1 + 1/Ri)^{0.5}} \tag{9b}$$

$$\sigma_{\theta i}^2 = c_\theta S_\theta^2 \ \frac{(1 + c_r / Ri)}{(1 + 1/Ri)} \tag{9c}$$

$$\sigma_{qi}^2 = c_q S_q^2 \ \frac{(1 + c_r / Ri)}{(1 + 1/Ri)} \tag{9d}$$

$$C_{\theta qi} = c_{\theta q} S_\theta S_q \ \frac{(1 + c_r / Ri)}{(1 + 1/Ri)} \tag{9e}$$

$$\sigma_{wi}^2 = c_w S_w^2 (1 + c_r/Ri) \tag{9f}$$

where H and Q are temperature and humidity fluxes, $\sigma_\theta^2, \sigma_q^2$, σ_w^2 are temperature, humidity, and vertical velocity variances, $C_{\theta q}$ is the temperature-humidity covariance, the index "i" refers to a value at the top of the mixed layer, and c_H , c_Q , c_θ , c_q , $c_{\theta q}$, c_w , c_r are universal constants (the same during both free and force convection). In this Section, the above expressions will be tested, based on the results of the LES model. Specifically, the dependence on the interfacial Richardson number will be examined.

Figure 6 shows the values of the dimensionless entrainment heat flux $H_i/(S_w S_\theta)$, obtained from the LES model (points), as a function of the interfacial Richardson number Ri. As expected, the negative values of the dimensionless entrainment heat flux increase when Ri decreases, and decrease when Ri increases. In the figure, the run names are indicated next to each point. The curve in the figure represents Equation (9a), plotted for $c_H = -0.0075$, and $c_r = 1.8$. The first constant has the same value as in the shear-free case (Sorbjan, 2005), and the second one as received by Sorbjan (2004).

Figure 7 shows that the values of the dimensionless entrainment humidity flux $Q_i/(S_w S_q)$, obtained from the LES (points) model as a function of Ri. In the figure, the dimensionless flux described by Equation (9c) is shown as a curve plotted for $c_Q = 0.0225$, and $c_r = 1.8$. The first constant has the same value as obtained by Sorbjan (2005) in the shear-free case. The second constant has the same value as obtained for the temperature flux.

Note that Eqs. 9a and 9b can be considered as alternative to Lilly's (1969) classical (zero-order) expressions for the entrainment heat, for the case when the interfacial layer has a finite depth. The zero-order model was originally derived for the stratocumulus-topped ABL, with a sharp temperature jump $\Delta\Theta$ and infinitesimal interfacial layer. Lilly's parameterization does not include any direct dependence on shear or Ri.

A simple condition (the humidity flux ratio Q_i/Q_o larger or smaller than unity) for the presence of moistening or drying regimes in the mixed layer can be obtained based on Equation (9b). If $Q_i/Q_o > 1$, or equivalently $R = -S_q/q_*(1+1.8/Ri)/(1+1/Ri)^{1/2} > c_Q^{-1} = 45$, the mixed layer will be dried, otherwise the mixed layer will be moistened. Based on Tables 1 and 2 it can be obtained that R equals 121.3 in run W05, R = 131.5 in run W10, and R = 149.6 in run W15,

which indicates drying. The values of R are: 41.7 in run S05, 21.8 in run S10, and 41.0 in run S15, which indicates moistening.

The peak values of the dimensionless temperature variance $\sigma_{\theta i}^2/S_\theta^2$ in the interfacial layer, obtained from the LES model, are displayed in Figure 8. In the figure, the dimensionless variance, estimated based on Equation (9b), is represented by a curve. The curve is plotted for $c_\theta = 0.040$, and $c_r = 8$. The first constant has the same value as obtained by Sorbjan (2005) in the shear-free case. The second constant is larger than the value 1.8 accepted by Sorbjan (2004).

The peak values of the dimensionless humidity variance σ_{qi}^2/S_q^2 in the interfacial layer, obtained from the LES model (points), are displayed in Figure 9. The obtained results reveal that the dimensionless variance strongly increases when Ri decreases, and decreases when Ri increases. In the figure, the variance, estimated based on Equation (9d), is also presented as a curve. The curve is plotted for constants: $c_q = 0.080$, and $c_r = 8$. The first constant is smaller than the value 0.175, accepted Sorbjan (2005) in the shear-free case. The second constant is larger than the value 1.8 accepted by Sorbjan (2004).

The peak values of the dimensionless temperature-humidity covariance $C_{\theta qi}/(S_\theta S_q)$ in the interfacial layer, obtained from the LES model (points), are displayed in Figure 10. The covariance strongly increases, when Ri decreases, and decreases when Ri increases. In the figure, the covariance, estimated based on Equation (9e), is also presented as a curve. The curve is plotted for constants: $c_{\theta q} = 0.050$, and $c_r = 8$. The first constant is smaller than the value 0.010 accepted Sorbjan (2005) in the shear-free case.

Figure 11 depicts the values of the dimensionless vertical velocity variance σ_{wi}^2/S_w^2 in the interfacial layer, obtained from the LES model (points). The obtained results show that σ_{wi}^2/S_w^2 increases, when Ri decreases, and decreases when Ri increases. In the figure, the dimensionless

variance, estimated based on Equation (9f), is represented as a curve. The curve is plotted for constants: $c_w = 0.040$, and $c_r = 8$. The first constant is smaller than the value 0.050 obtained by Sorbjan (2005) in the shear-free case. For the second constant is larger than the value 1.8 obtained by Sorbjan (2004).

One should be aware of uncertainty concerning the results of large-eddy simulations, due to a numerical effects, resolution, and sub-grid parameterization. Therefore, the constants, obtained in this study, require further verification based on LES experiments with higher resolution, and also on atmospheric data.

4. Parameterization

Based on Equations (5) and (9), and the results discussed in Section 3.2, the following expressions can be proposed for profiles of scalar moments in the atmospheric boundary layer with shear:

$$H = w_* \Theta_* \ (1 - z/z_i) - c_H S_w S_\theta \ \frac{(1 + c_{rH}/Ri)}{(1 + 1/Ri)^{0.5}} \ z/z_i \tag{10a}$$

$$Q = w_* q_* \ (1 - z/z_i) - c_Q S_w S_q \ \frac{(1 + c_{rQ}/Ri)}{(1 + 1/Ri)^{0.5}} \ z/z_i \tag{10b}$$

$$\sigma_\theta^2 = c_1 \ \Theta_*^{\,2} \frac{(1 - z/z_i)}{(z/z_i)^{2/3}} + c_\theta S_\theta^2 \ \frac{(1 + c_r/Ri)}{(1 + 1/Ri)} \ \frac{(z/z_i)^9}{(2.05 - z/z_i)^8} \tag{10c}$$

$$\sigma_q^2 = c_2 \ q_*^{\,2} \frac{(1 - z/z_i)^8}{(z/z_i)^{2/3}} + c_q S_q^2 \ \frac{(1 + c_r/Ri)}{(1 + 1/Ri)} \left[\frac{(z/z_i)^3}{(2.2 - z/z_i)^5} + c_s \right] \tag{10d}$$

$$C_{\theta q} = c_3 \ \Theta_* q_* \frac{(1 - z/z_i)}{(z/z_i)^{2/3}} + c_{\theta q} S_\theta S_q \ \frac{(1 + c_r/Ri)}{(1 + 1/Ri)} \ \frac{(z/z_i)^8}{(2.2 - z/z_i)^8} \tag{10e}$$

$$\sigma_w^{\,2} = 1.4 \ c_3 \ (1\text{-}z/z_i)^{4/3} (z/z_i)^{2/3} + c_w S_w^{\,2} (1 + c_r/Ri) \ (z/z_i)^{1/2} \ (1.1 - z/z_i)^{1/3} \tag{10f}$$

Note that for given scales w_*, Θ_*, q_*, S_w, S_θ, S_q, and for Ri, the proposed functions of z/z_i in (10a-f) are arbitrary curves fitting the obtained LES results. Their form is the same as in the free-convection case, when 1/Ri = 0 (Sorbjan, 2005). The above expressions are valid below the level, at which a moment has its peak, and above the surface layer (even thought the dependence on height for small z seems to follows the surface-layer predictions).

For the purpose of illustration, the curves described by Equations (10c), (10d) and (10e) are compared with the LES profiles obtained in runs W10, W15, S10, and S15 in Figures 12 a-c. For clarity of the presentation, the logarithmic scale of abscissa is used in Figures 12 a-b. The curves are plotted for the values of parameters Ri, S_θ/Θ_* and S_q/q_* displayed in Table 1 and 2, and for the following values of constants, obtained in Section 3.2: $c_1 = 0.95$, $c_2 = 1$, $c_3 = 1.5$, $c_\theta = 0.04$, $c_q = 0.08$, $c_{\theta q} = 0.1$, $c_r = 8$, $c_s = 0.02$. As mentioned in Section 3.2, the values of c_1, c_2, c_3, and $c_{\theta q}$ are the same as used in the shear-less case by Sorbjan (2005). The values of c_q, c_s, and c_r differ from the values employed in Part I.

Figure 12a indicates that in the lower part of the mixed layer, the LES curves (continuous lines) for of the dimensionless temperature variance, and the approximating profiles (broken lines), are nearly identical. Above, the approximating profiles diverge at $z/z_i = 0.5$, depending on the temperature stratification in the interfacial layer. The LES curves show the same trend, but above $z/z_i = 0.9$.

The dimensionless humidity variances, obtained from Eq. 10d (thick broken lines), reproduce the tendency of the LES curves: the S10 and S15 profiles (thick continuous lines) in Figure 12b are shifted along abscissa to the left (toward smaller values), while the W10 and W15 profiles are shifted to the right. When the geostrophic wind G increases, the profiles are shifted along abscissa toward larger values.

The LES curves and approximating profiles of the dimensionless temperature-humidity covariances, in Figure 12c, are nearly identical in the lower part of the mixed layer. At the top of the mixed layer the combination of the governing parameters Ri, $S_{\theta i}/\Theta_*$ and S_{qi}/q_* causes that the LES curves and approximating profiles of all dimensionless temperature-humidity covariances, in Figure 12c, are relatively close to each other, except in case W15 (compare with Figure 4c. The presented results have a preliminary character. They require further verification based on LES experiments with finer resolution, and also on atmospheric data.

5. Concluding Remarks

The large-eddy simulation model has been used in this study to examine the impact of stratification and shear in the interfacial layer during forced convection. The performed LES tests show that in the upper portion of the mixed layer the dimensionless (in terms of mixed layer parameters given by Eqs. 2) vertical gradients of temperature, humidity, and wind velocity depend on the dimensionless height z/z_i and the Reech number Rn.

It is also confirmed that the interfacial layer is governed by a set of interfacial scales (2). The characteristic values of statistical moments of scalars at the top of the mixed layer during sheared convection, scaled by the interfacial scales (Eqs. 3), are shown to be functions of the interfacial Richardson number Ri, as predicted by Equations (9). Based on these findings, a parameterization (10) is proposed for profiles of scalar variances and covariances. The parameterization employs a combination of the mixed layer and interfacial scales, and two semi-empirical similarity functions F_m and F_i, which are dependent on the dimensionless height z/z_i, and on the Richardson number Ri. The obtained similarity expressions adequately approximate

the LES profiles of temperature and humidity statistics, and also properly represent the impact of stability, shear, and entrainment. When the effects of shear decrease ($1/Ri \rightarrow 0$), the derived equations take form of free-convection profiles obtained in Part 1 of this study (Sorbjan, 2005). As in the shear-free case, the humidity variance in the surface layer is controlled by entrainment, especially in the "drying" case, and do not seem to follow the Monin-Obuhkov similarity predictions.

Acknowledgements. The performed research has been supported by the National Science Foundation grant No. ATM-0400590.

References

Deardorff, J.W.: 1970, "Convective Velocity and Temperature Scales for the Unstable Planetary Boundary Layer and for Raleigh Convection". *J. Atmos. Sci.,* **27**, 1211-1213.

Deardorff, J.W.: 1974a, "Three-Dimensional Numerical Study of the Height and Mean Structure of a Heated Planetary Boundary". *Bound.-Layer Meteor*, **7**, 81-106.

Deardorff, J.W.: 1974b, "Three-Dimensional Numerical Study of Turbulence in an Entraining Mixed Layer". *Bound.-Layer Meteor*, **7**, 199-226.

Garratt, J.R.: 1992, *The atmospheric boundary layer*. Cambridge University Press, 316 pp.

Glendening, J.W.: 1996, "Linear Eddy Features Under Strong Shear Conditions". *J. Atmos. Sci.*, **53**, 3430-3449.

Lilly, D.K: 1968, "Models of Cloud-Topped Mixed Layers under Strong Inversion", *Quart. J. Roy.Meteor. Soc.,* **94**, 292-309.

Lilly, D.K: 2002, "Entrainment into Mixed Layers. Part I: Sharp-Edged and Smoothed Tops". *J. Atmos. Sci.*, **59**, 3340-3361.

Kim, S.-W., S.-U. Park, and C.-H. Moeng: 2003, "Entrainment Processes in the Convective Boundary Layer with Varying Wind Shear". *Bound.-Layer Meteor*, **108**, 221-245.

Mahrt, L.: 1991, "Boundary-layer moisture regimes". Q. J. R. Meteor. Soc, **117**, 151-176.

Mason, P.J.: 1992, "Large-Eddy Simulation of Dispersion in Convective Boundary Layer with Wind Shear". *Atmospheric Environment*, **26**, 9, 151-1571.

Moeng, C.H. and P.P. Sullivan: 1994, "A Comparison of Shear and Buoyancy Driven Planetary Boundary Layer Flows". *J. Atmos. Sci.,* **51** , 999-1022.

Otte M.J, and J.C. Wyngaard: 2000, "Stably Stratified Interfacial-layer Turbulence". in *14th Symposium on Boundary Layer and Turbulence. American Meteorological Society, Aspen*, pp.74-75.

Sorbjan, Z.:1991, "Evaluation of Local Similarity Functions in the Convective Boundary Layer". *J. Appl. Meteor.,* **30**, 1565-1583.

Sorbjan, Z.:1996, "Numerical Study of Penetrative and 'Solid Lid' Non-penetrative Convective Boundary Layers". *J. Atmos. Sci.*, **53**, 101-112.

Sorbjan, Z.:1999, "Similarity of Scalar Fields in the Convective Boundary Layer. *J. Atmos. Sci.,* **56**, 2212-2221.

Sorbjan, Z.:2001, "An evaluation of Local Similarity at the TOP of the Mixed Layer Based on Large-eddy Simulations". *Bound.-Layer Meteorol.*, **101**., 183-207.

Sorbjan, Z.:2004, "Large-eddy Simulations of the Baroclinic Mixed Layer". *Bound.-Layer Meteorol.*, **112**., 57-80.

Sorbjan, Z.:2005, "Statistics of Scalar Fields in the Atmospheric Boundary Layer Based on

Large-Eddy Simulations. Part I: Free convection". Accepted to *Bound.-Layer Meteorol.*

Sullivan, P.T., T.W. Horst, D.H. Lenschow, C.-H. Moeng, and J.C. Weil: 2003, "Structure of Subfilter-Scale Fluxes in the Atmospheric Surface Layer with Application to LES Modeling". *J. Fluid. Mech.,* **482**, 101-139.

Wyngaard, J.C., O.R. Cote, and Y. Izumi.:1971, "Local Free Convection, Similarity and Budgets of Shear Stress and Heat Flux". *J. Atmos. Sci.*, **28**, 1171-1182.

Figure captions

Figure 1. Vertical profiles of: (a) potential temperature, (b) humidity, and (c) velocity components in all performed simulations

Figure 2. Dimensionless gradients of: (a) temperature $z_i/\Theta_*\, d\Theta/dz$, (b) humidity $z_i/q_*\, dq/dz$, and (c) the x-component of the wind velocity vector $z_i/u_*\, du/dz$, obtained in runs W10, S10, and W15, S15.

Figure 3. Dimensionless profiles of: (a) potential temperature flux H/H_o, (b) potential temperature variance $\sigma_\theta^2/\Theta_*^2$, obtained in runs W10, W15, and S10, S15.

Figure 4. Dimensionless profiles of: (a) humidity flux Q/Q_o, (b) humidity variance σ_q^2/q_*^2, (c) temperature-humidity covariance $C_{\theta q}/(\Theta_* q_*)$, obtained in runs W10, S10, and W15, S15.

Figure 5. Dimensionless velocity variances: (a) horizontal σ_u^2/w_*^2, and (b) vertical σ_w^2/w_*^2, obtained in runs W10, S10, and W15, S15.

Figure 6. The dimensionless heat flux $H_i/(S_w S_\theta)$, obtained from the LES model (dark circles), as a function of the interfacial Richardson number Ri. In the figure, Eq. 6a is represented by a curve. The LES run names are indicated next to each point.

Figure 7. The dimensionless humidity flux $Q_i/(S_w S_q)$, obtained from the LES model (dark circles), as a function of the interfacial Richardson number Ri. In the figure, Eq. 6b is represented by a curve. The LES run names are indicated next to each point.

Figure 8. The dimensionless temperature variance $\sigma_{\theta i}^2/S_\theta^2$, obtained from the LES model (dark circles), as a function of the interfacial Richardson number Ri. In the figure, Eq. 6c is represented by a curve. The LES run names are indicated next to each point.

Figure 9. The dimensionless humidity variance σ_{qi}^2/S_q^2, obtained from the LES model (dark circles), as a function of the interfacial Richardson number Ri. In the figure, Eq. 6d is represented by a curve. The LES run names are indicated next to each point.

Figure 10. The dimensionless temperature-humidity covariance $C_{\theta qi}^2/(S_\theta S_q)$, obtained from the LES model (dark circles), as a function of the interfacial Richardson number Ri. In the figure, Eq. 6e is represented by a curve. The LES run names are indicated next to each point.

Figure 11. The dimensionless vertical velocity variance σ_{wi}^2/S_w^2, obtained from the LES model (dark circles), as a function of the interfacial Richardson number Ri. In the figure, Eq. 6f is represented by a curve. The LES run names are indicated next to each point.

Figure 12. Comparison of the LES curves, obtained in runs S10, S15 (thick lines), and W10, W15, with analytical profiles (broken lines) of: (a) the dimensionless potential temperature variance $\sigma_\theta^2/\Theta_*^2$, obtained from Eq.10c, (b) the dimensionless humidity variance σ_q^2/q_*^2, obtained from Eq. 10d, (c) the dimensionless temperature-humidity covariance $C_{\theta q}/\Theta_* q_*$, obtained from Eq. 10e.

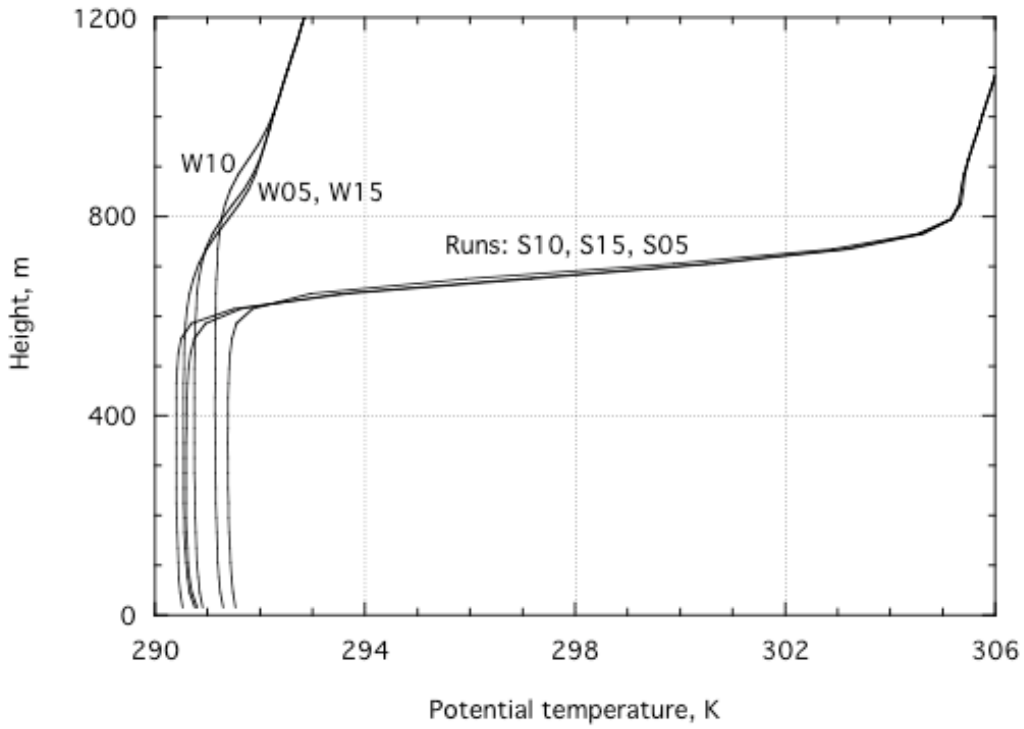
1200
800
400
0
Height, m
290
294
298
302
306
Potential temperature, K
W10
W05, W15
Runs: S10, S15, S05

Figure 1a

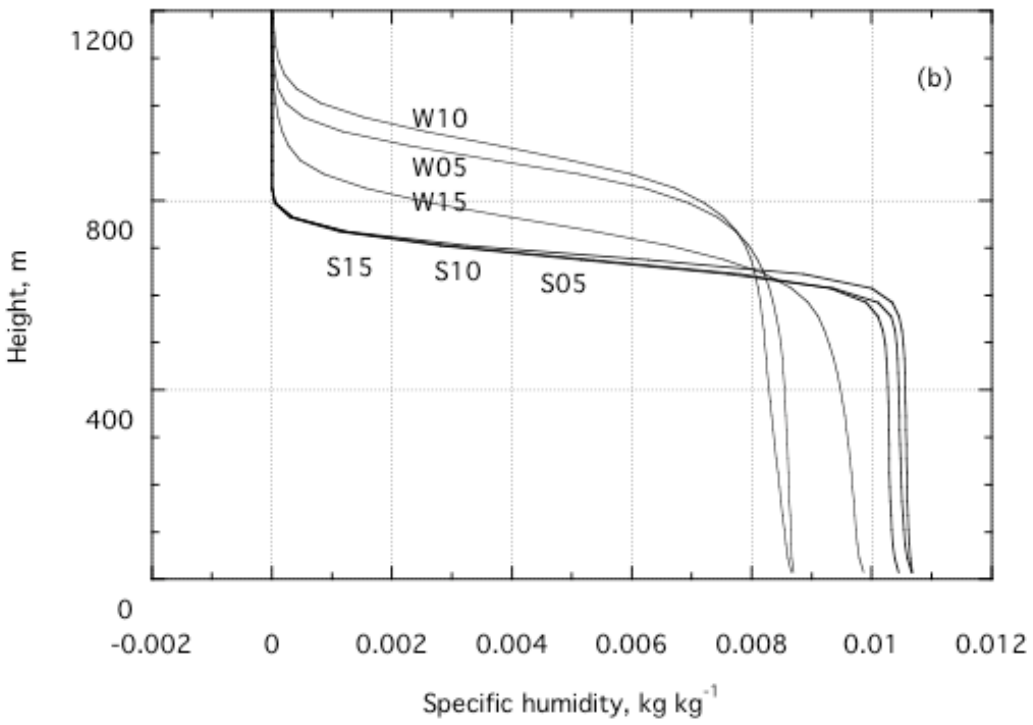
(b)
W10
W05
W15
S15
S10
S05
1200
800
400
0
Height, m
-0.002
0
0.002
0.004
0.006
0.008
0.01
0.012
Specific humidity, kg kg-1

Figure 1b

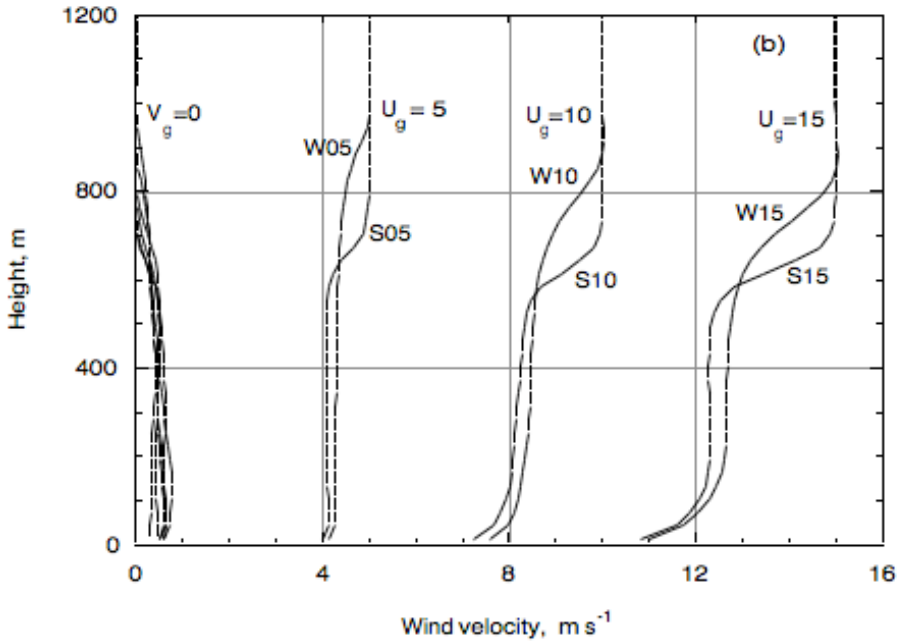
1200
800
400
0
Height, m
0
4
8
12
16
Wind velocity, m s-1
(b)
Vg=0
Ug = 5
W05
S05
Ug=10
W10
S10
Ug=15
W15
S15

Figure 1c

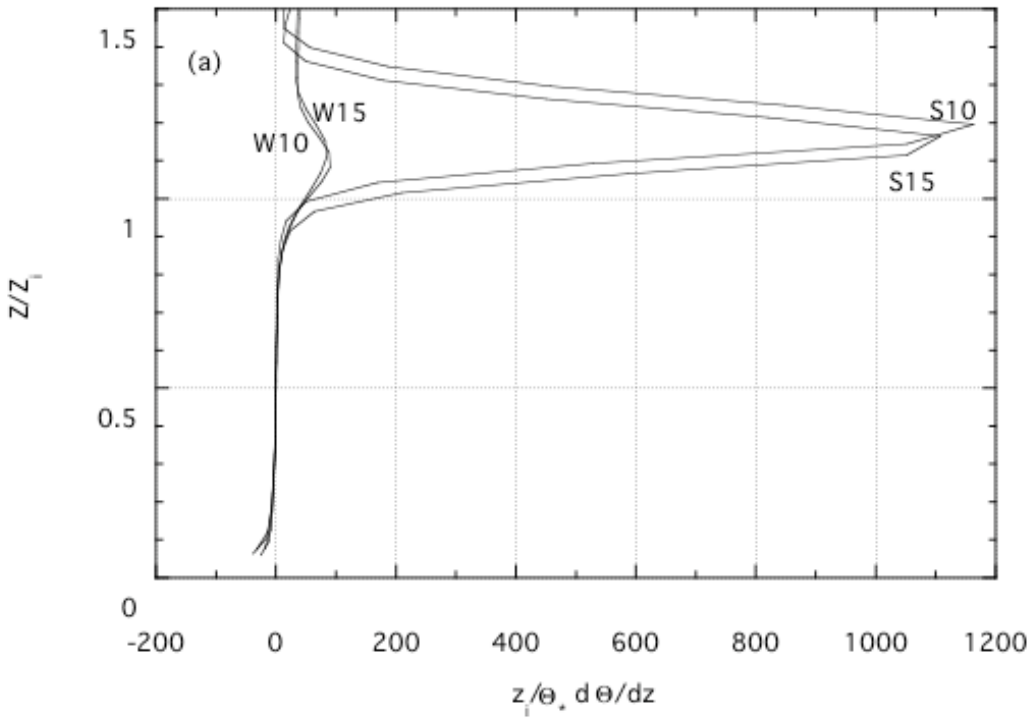
(a)
W15
W10
S10
S15
1.5
1
0.5
0
z/z_i
-200
0
200
400
600
800
1000
1200
z_i/Θ_* dΘ/dz

Figure 2a

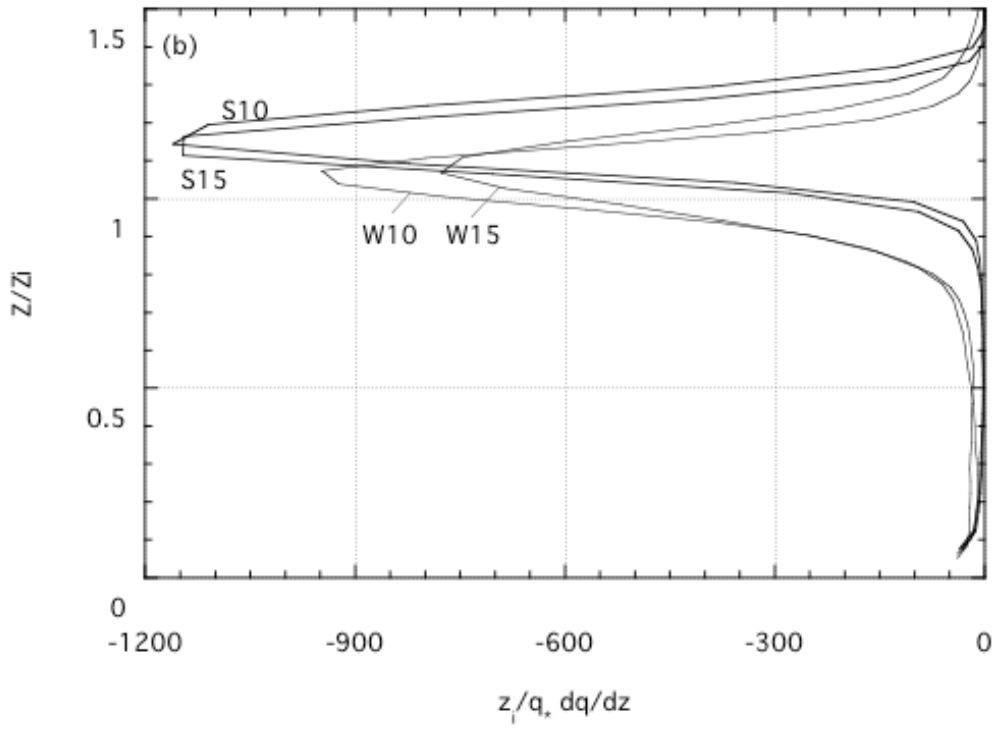

Figure 2b

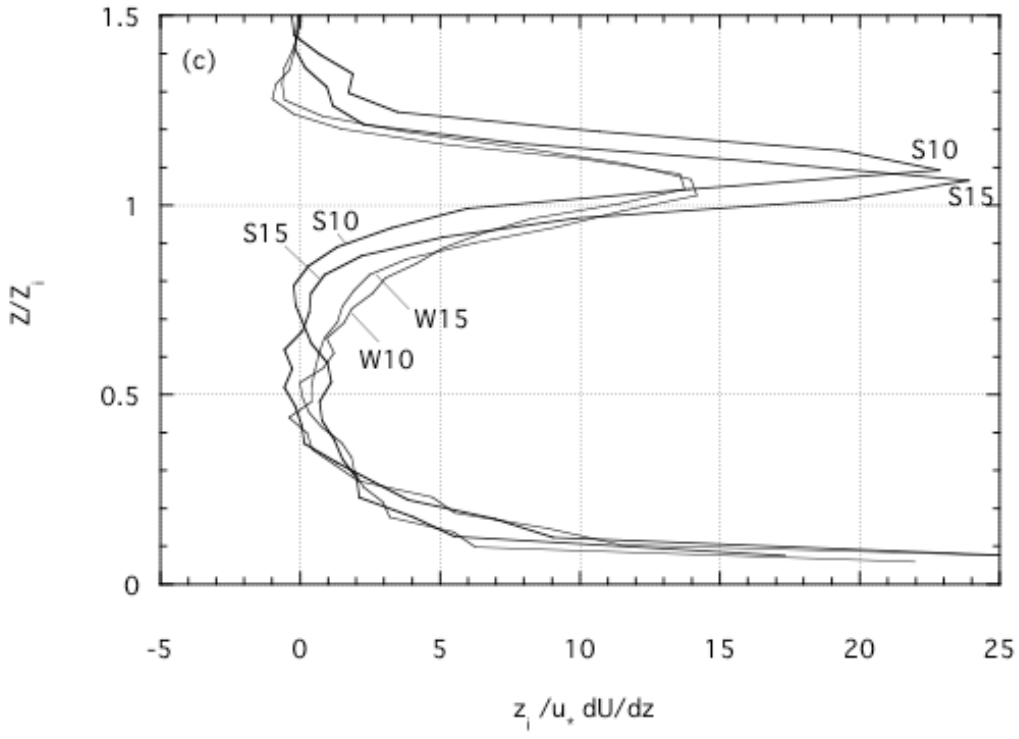

Figure 2c

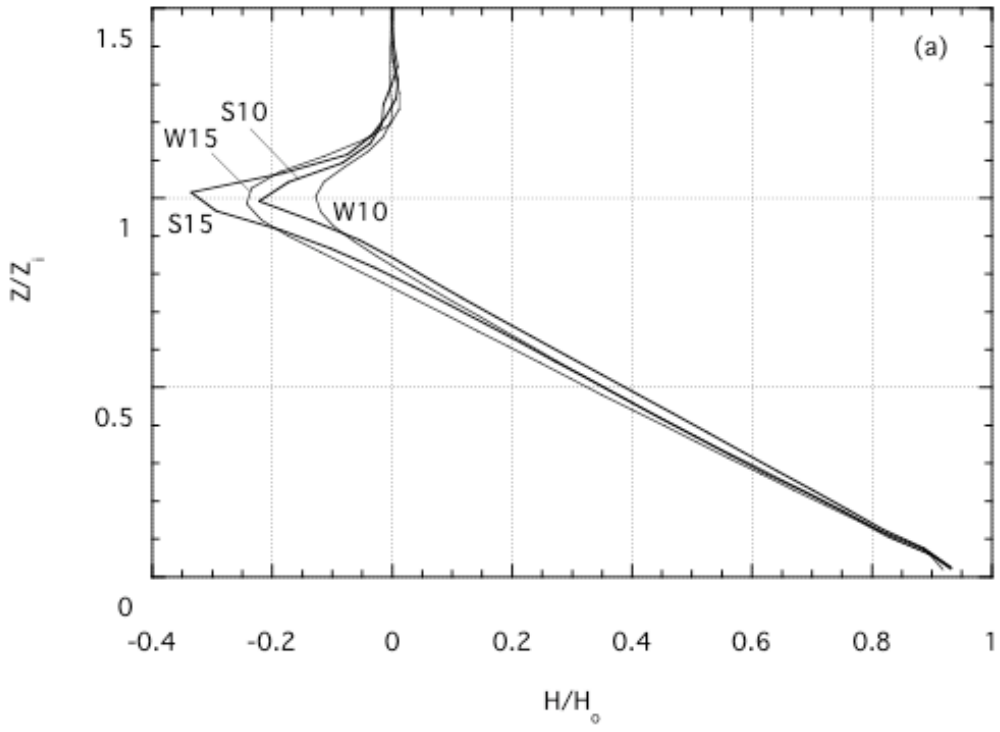

Figure 3a

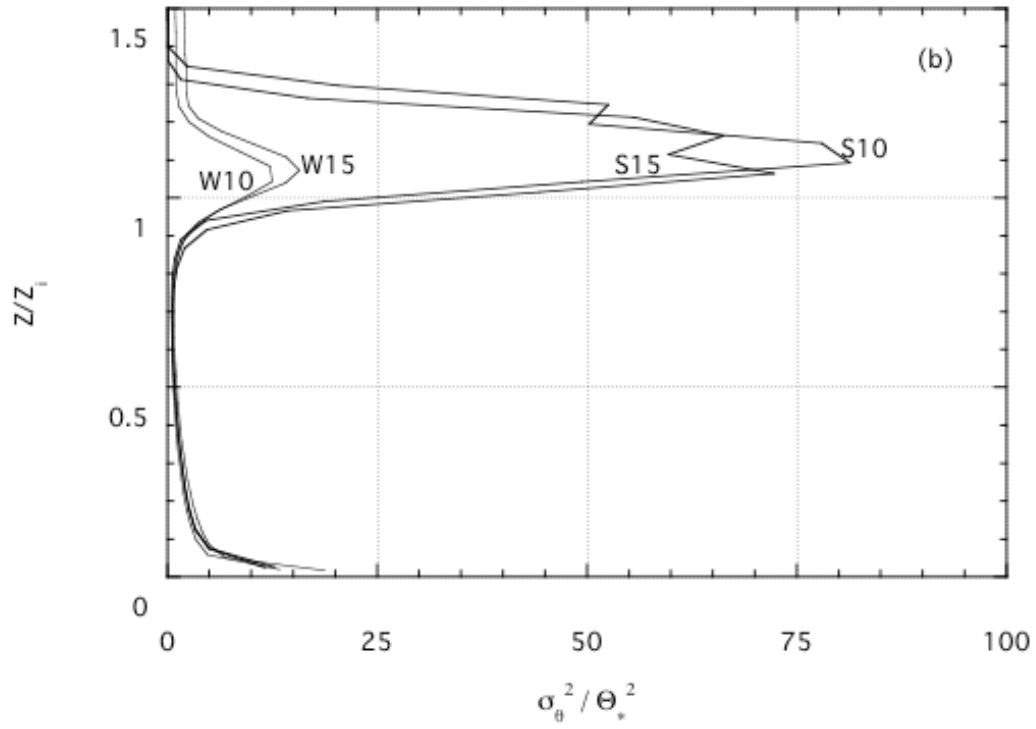

Figure 3b

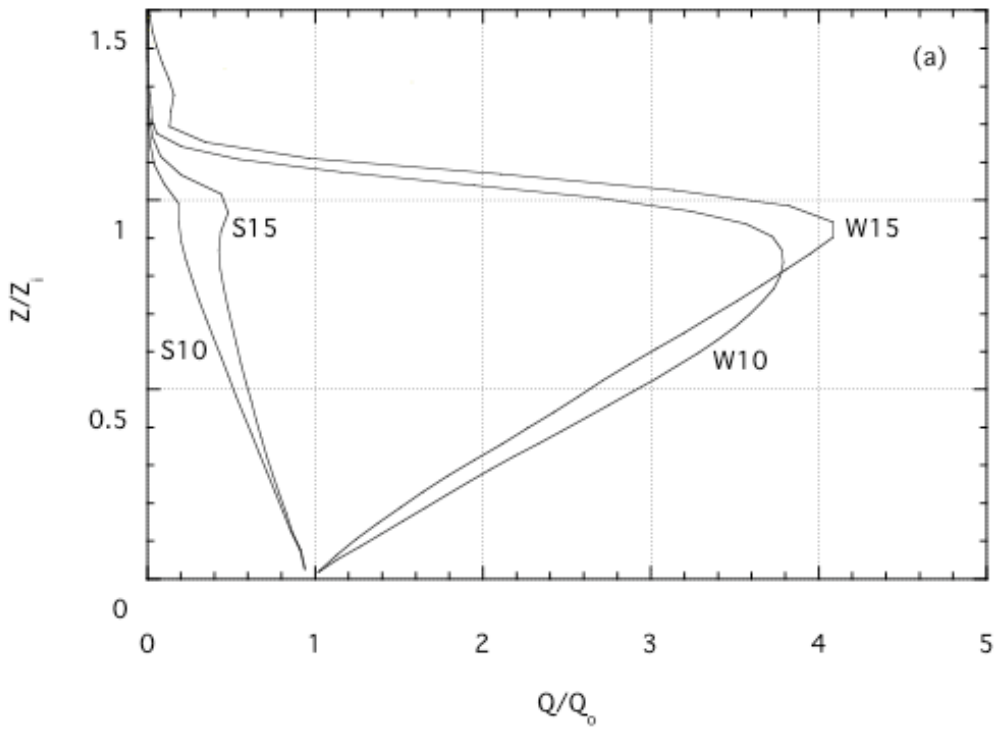

Figure 4a

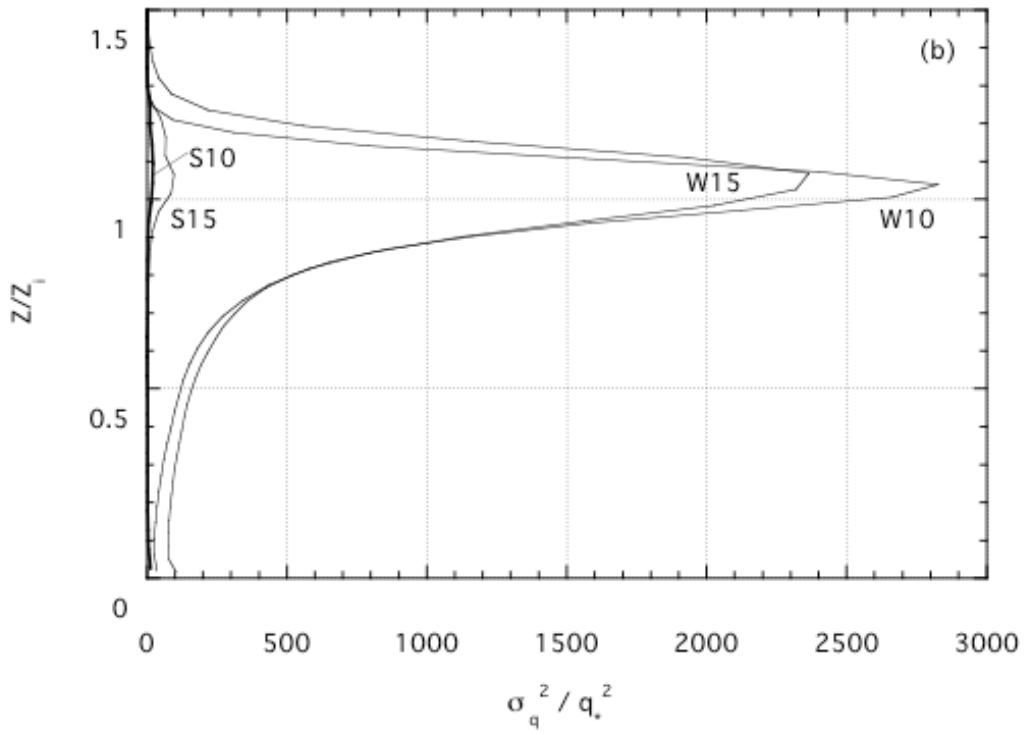
(b)
S10
S15
W15
W10
1.5
1
0.5
0
0
500
1000
1500
2000
2500
3000
Z/Z_i
σ_q² / q_*²

Figure 4b

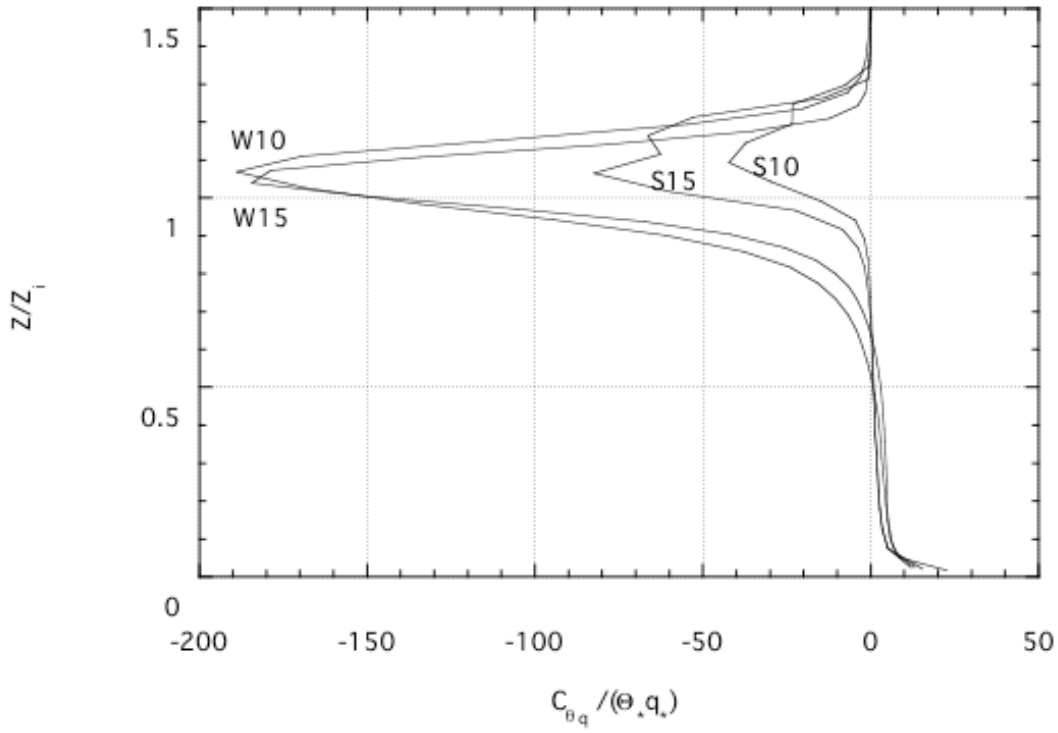

Figure 4 c.

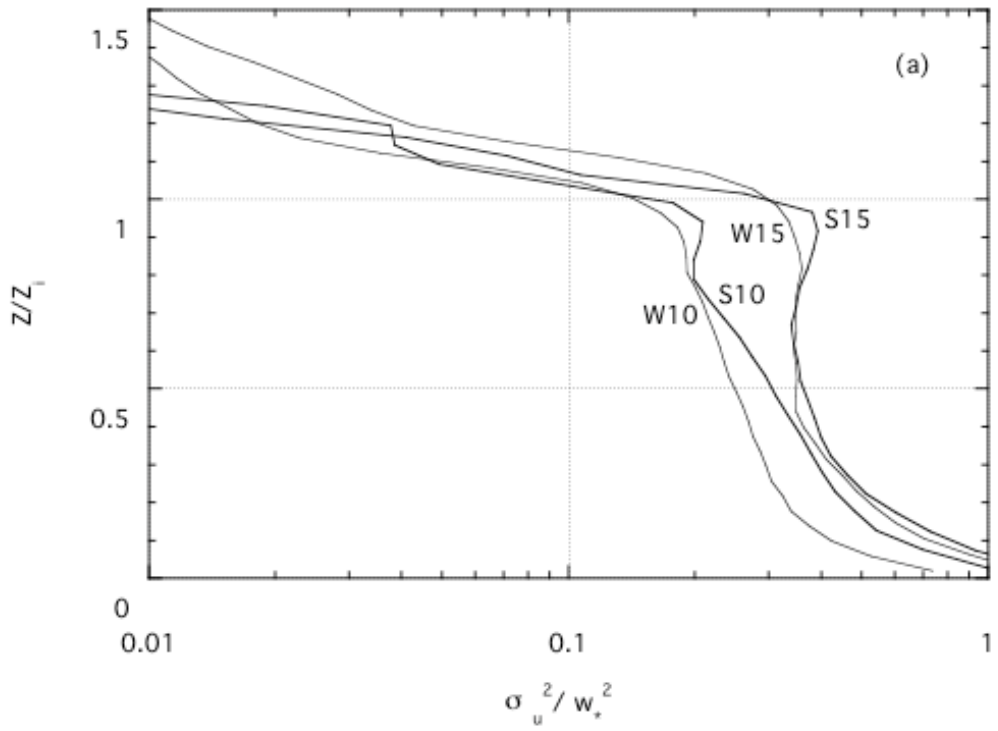

Figure

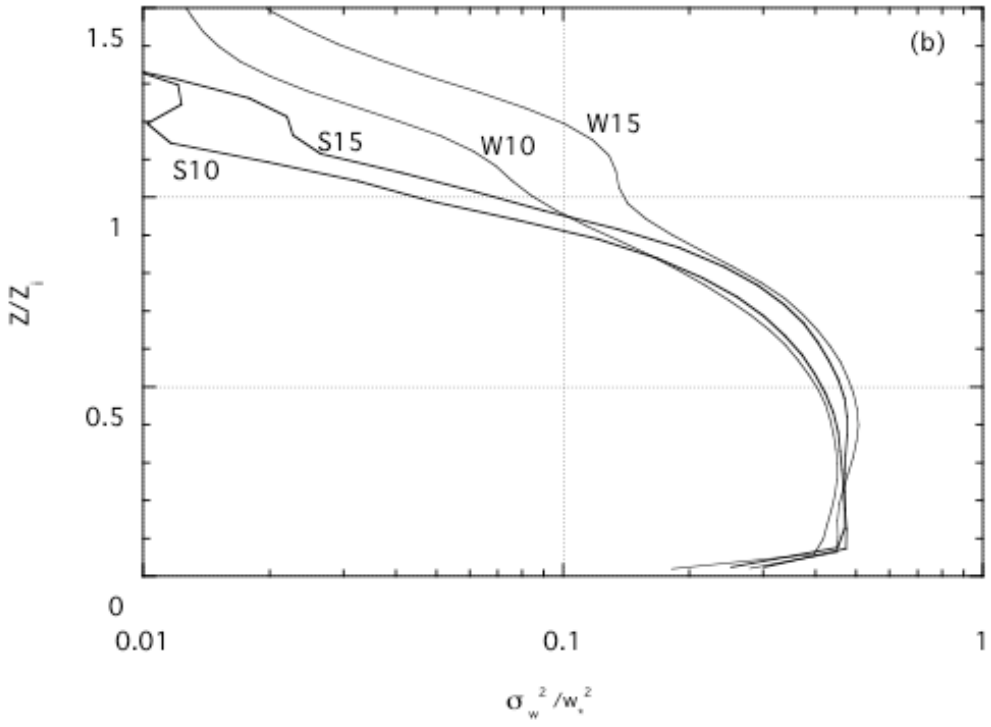

Figure 5b

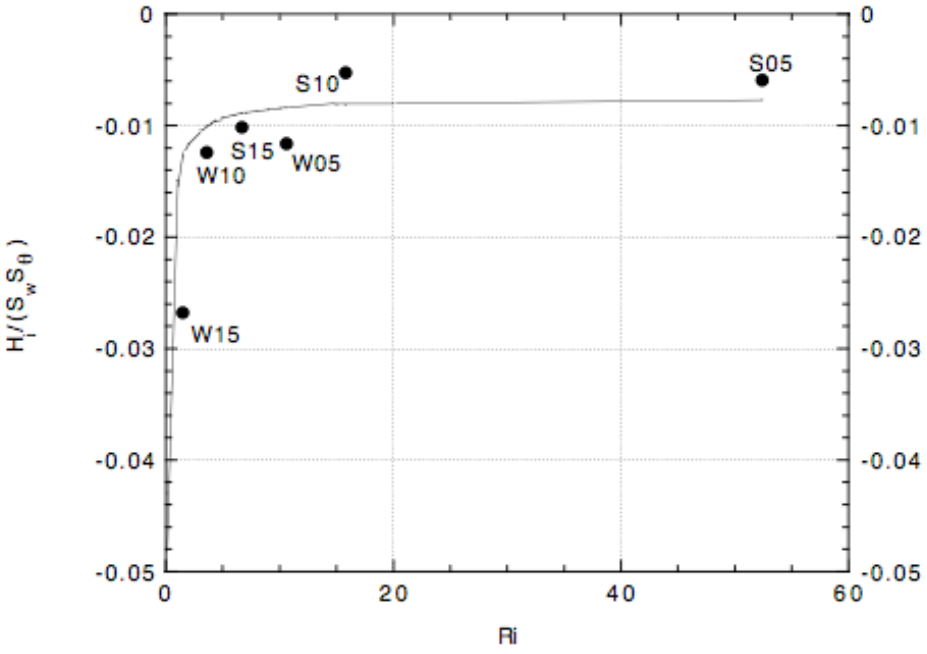
0
-0.01
-0.02
-0.03
-0.04
-0.05
0
20
40
60
Ri
$H_l/(S_w S_\theta)$
S10
S05
S15
W05
W10
W15

Figure 6

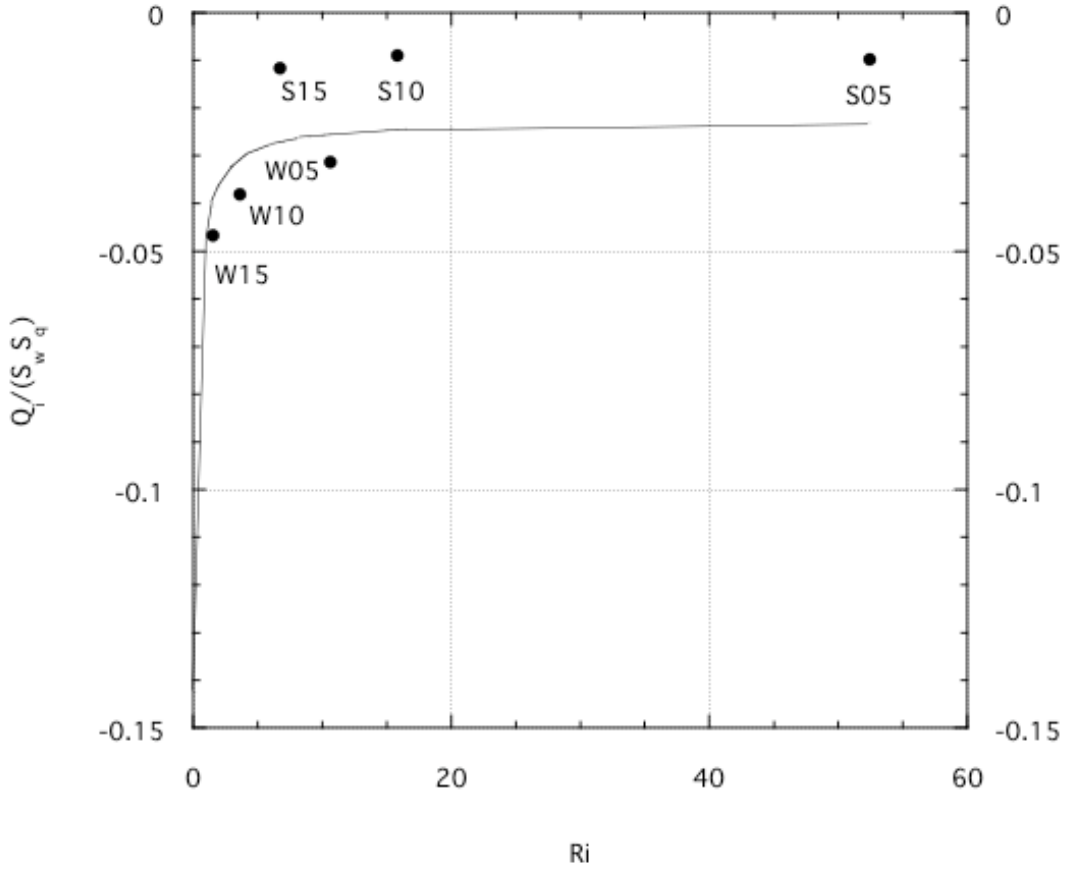

Figure 7

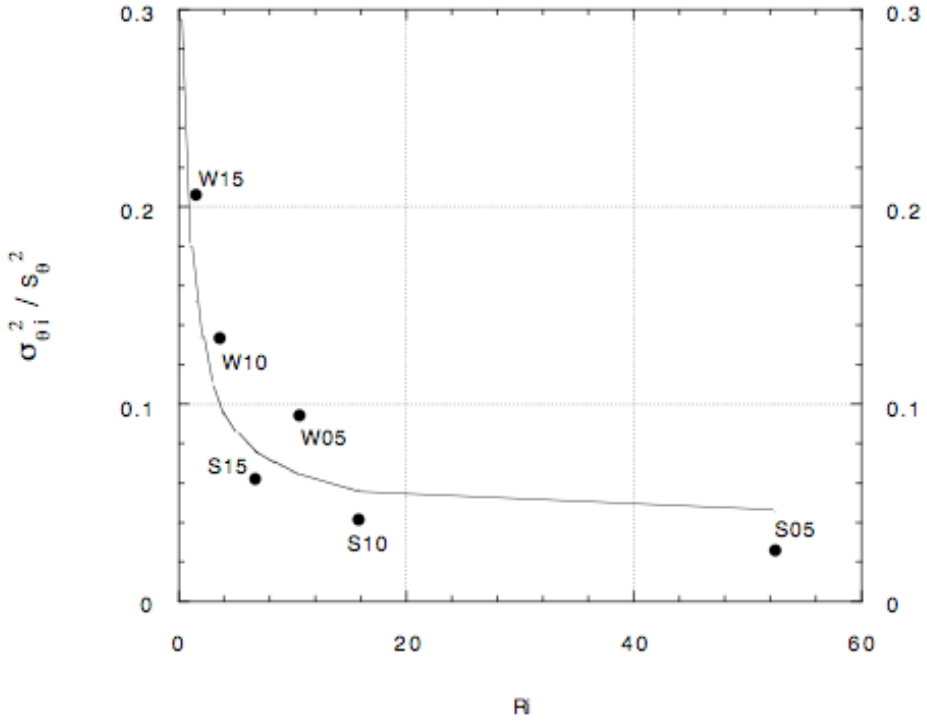
0.3
0.2
0.1
0
0.3
0.2
0.1
0
W15
W10
W05
S15
S10
S05
0
20
40
60
Ri
$\sigma_{\theta i}^2 / s_\theta^2$

Figure 8

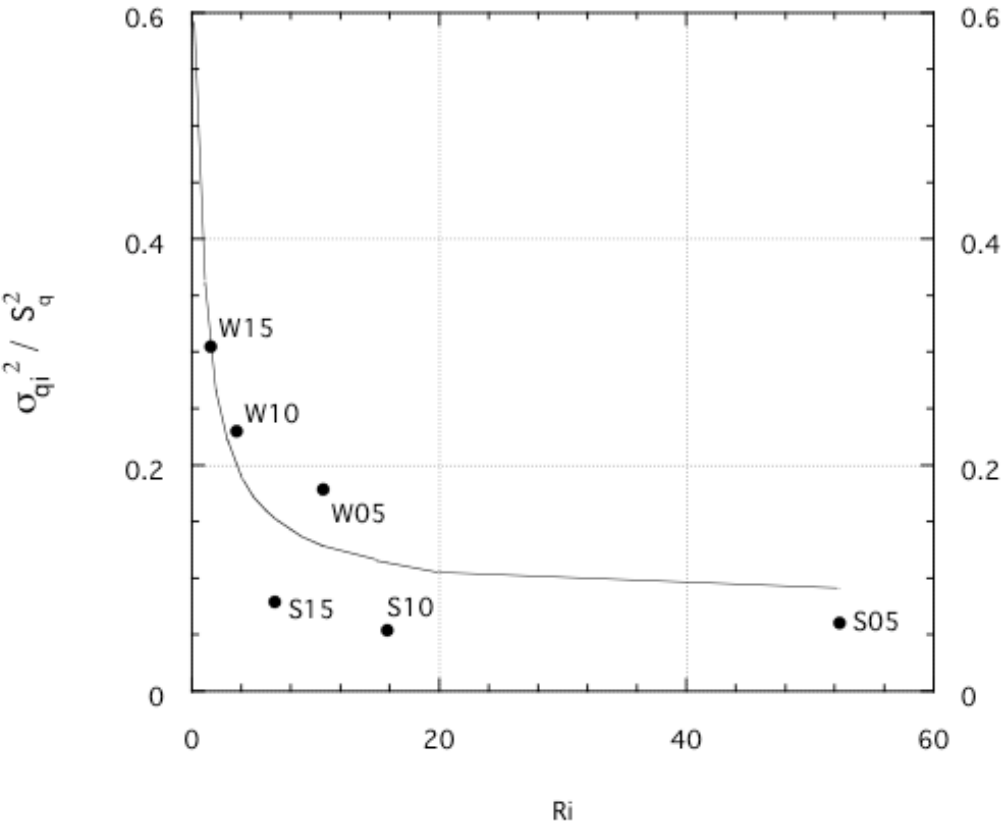

Figure 9

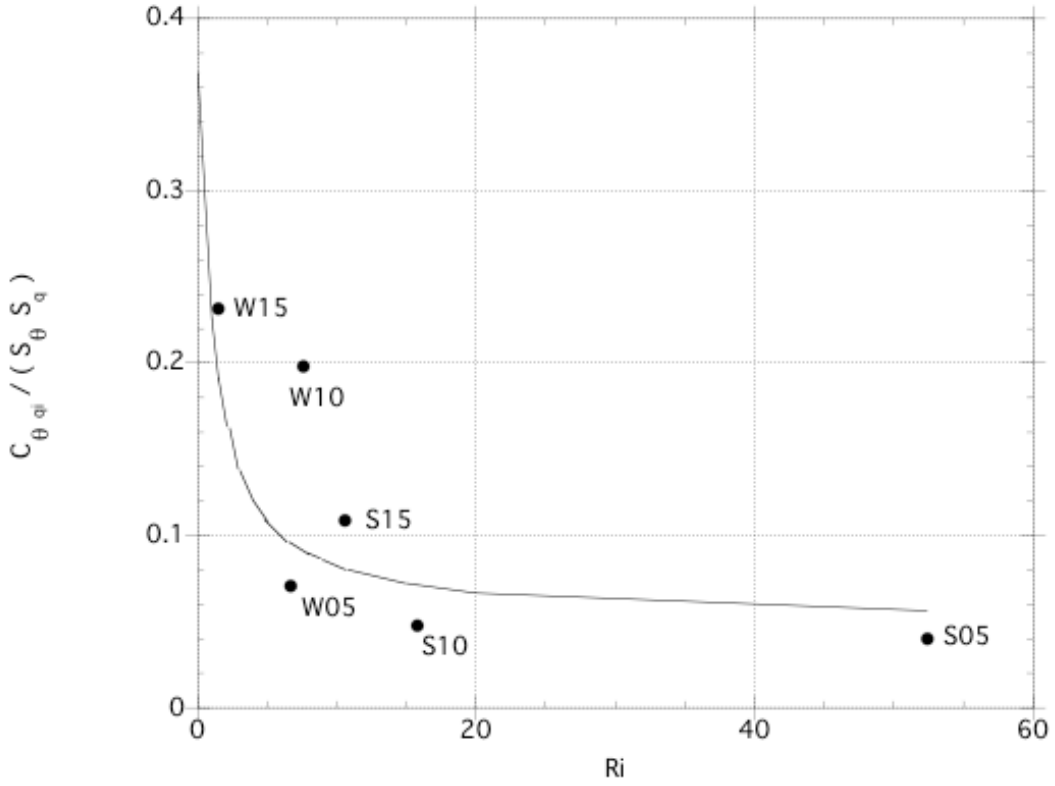
0.4
0.3
0.2
0.1
0
0
20
40
60
Ri
$C_{\theta q} / (S_\theta S_q)$
W15
W10
S15
W05
S10
S05

Figure 10

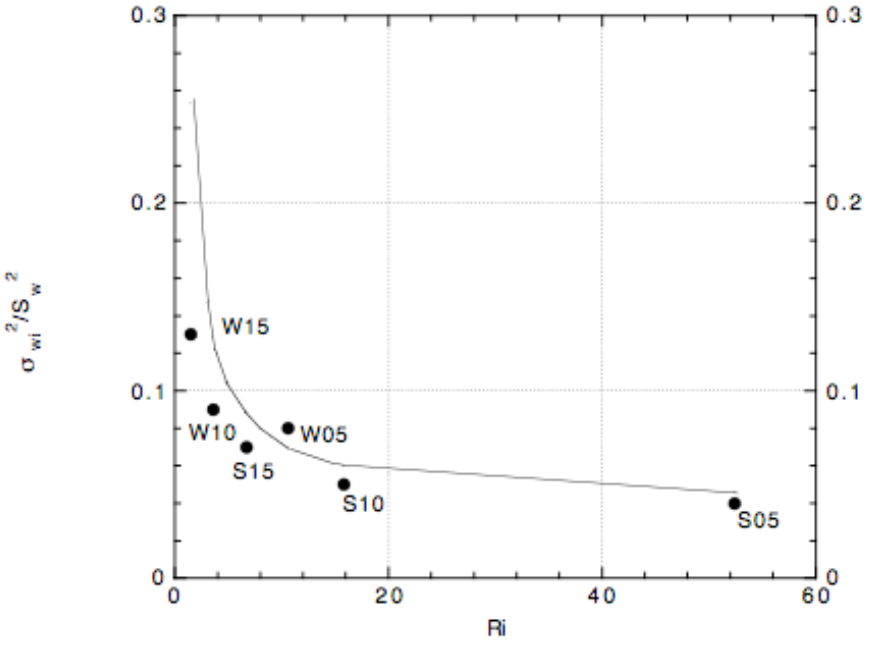

Figure 11

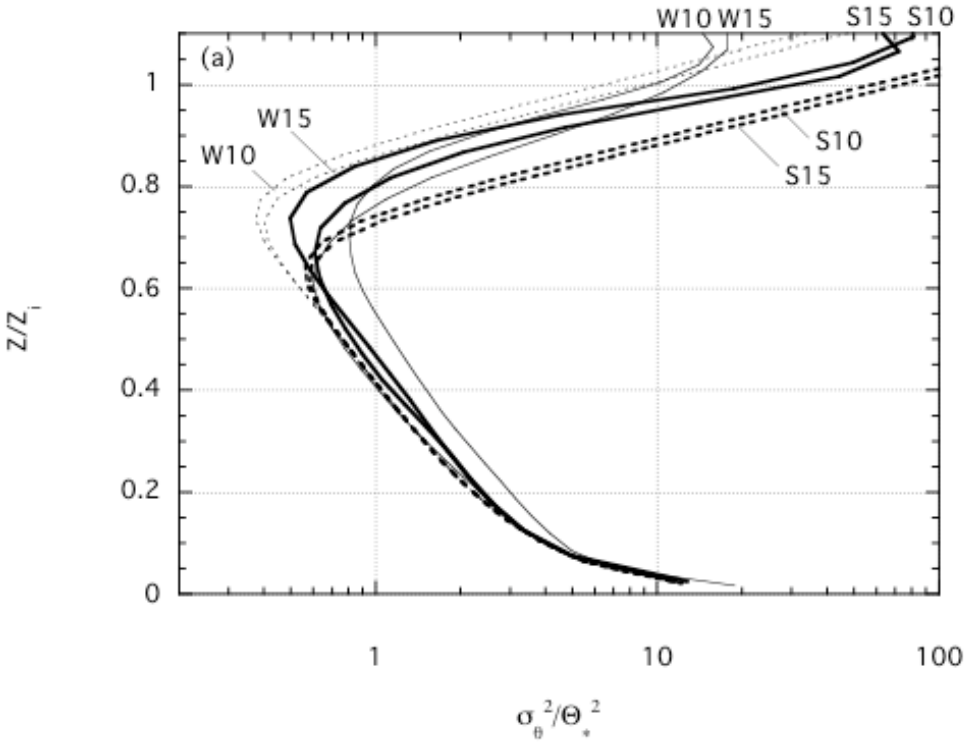

Figure 12a

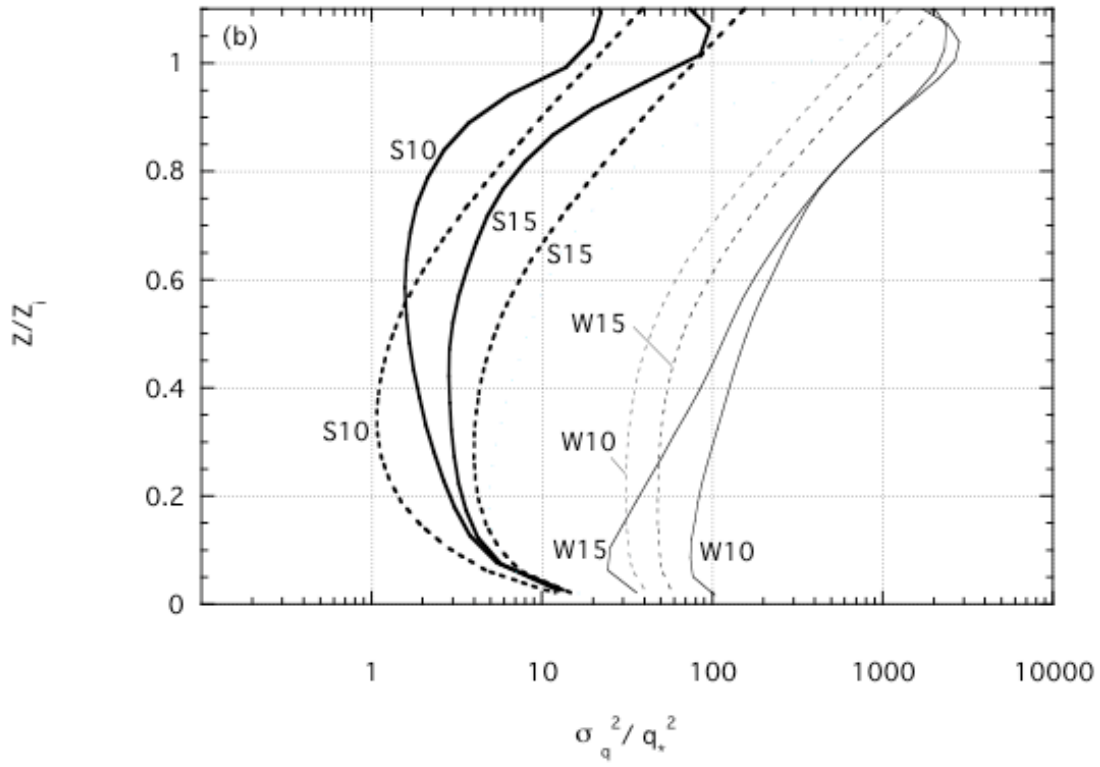
(b)
S10
S15
S15
W15
W10
S10
W15
W10
1
0.8
0.6
0.4
0.2
0
z/z_i
1
10
100
1000
10000
σ_q^2 / q_*^2

Figure 12b

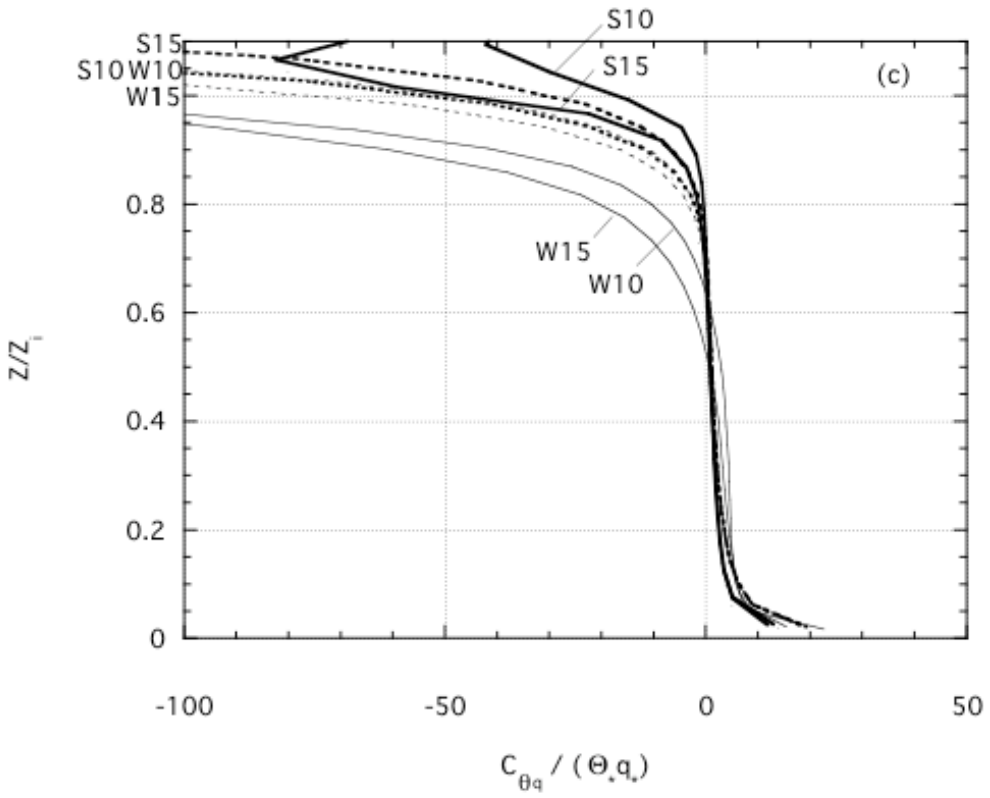
S10
S15
S10W10
W15
S15
(c)
W15
W10
0.8
0.6
0.4
0.2
0
Z/Z_i
-100
-50
0
50
C_θq / (Θ_* q_*)

Figure 12c